Comprehensive model of electromigrative transport in microfluidic paper based analytical devices

Federico Schaumburg[1], Pablo A. Kler[2,3], and Claudio L. A. Berli[1]

[1]INTEC (Universidad Nacional del Litoral–CONICET), Colectora RN 168 Km 472, S3000GLN Santa Fe, Argentina.
[2]CIMEC (Universidad Nacional del Litoral–CONICET), Colectora RN 168 Km 472, S3000GLN Santa Fe, Argentina.
[3]Departamento de Ingeniería en Sistemas de Información, FRSF-UTN., Lavaise 610, S3004EWB Santa Fe, Argentina.

Prof. Dr. Claudio L.A. Berli
Instituto de Desarrollo Tecnológico para la Industria Química
Universidad Nacional del Litoral–CONICET
Colectora RN 168 Km 472, S3000GLN Santa Fe, Argentina.
Tel: +54-342-4511594 ext 1010.
Fax: +54-342-4511169
email: cberli@santafe-conicet.gov.ar. ORCID ID: http://orcid.org/0000-0002-1321-6738

List of abbreviations:

EDMSD	Electrophoretically-driven mechanical solute dispersion
μPAD	Microfluidic paper-based analytical device
FEM	Finite element method
FFE	Free-flow electrophoresis
FFEIEF	Free-flow IEF
FVM	Finite volume method
FWHM	Full width at half maximum
LE	Leading electrolyte
PDE	Partial differential equation
TE	Trailing electrolyte
ZE	Zone electrophoresis

Keywords: Electroosmotic flow; Electrophoresis; Mathematical modelling; Paper based microfluidics; Transport phenomena.

Abstract

A complete mathematical model for electromigration in paper-based analytical devices is derived, based on differential equations describing the motion of fluids by pressure sources and EOF, the transport of charged chemical species and the electric potential distribution. The porous medium created by the cellulose fibers is considered like a network of tortuous capillaries and represented by macroscopic parameters following an effective medium approach. The equations are obtained starting from their open-channel counterparts, applying scaling laws and, where necessary, including additional terms. With this approach, effective parameters are derived, describing diffusion, mobility and conductivity for porous media. While the foundations of these phenomena can be found in previous reports, here, all the contributions are analyzed systematically and provided in a comprehensive way. Moreover, a novel electrophoretically driven dispersive transport mechanism in porous materials is proposed. Results of the numerical implementation of the mathematical model are compared with experimental data, showing good agreement and supporting the validity of the proposed model. Finally, the model succeeds in simulating a challenging case of free-flow electrophoresis in paper, involving capillary flow and electrophoretic transport developed in a 2D geometry.

1 Introduction

Electrophoresis on paper substrates was first studied 70 years ago, where the most outstanding works where those from Tiselius on serum protein separation [1, 2]. Electrophoresis then evolved using more uniform media, like gel [3, 4] and open (i.e. non-porous) channels, like glass and fused-sillica capillaries [5, 6]. More recently, the technique was integrated to microfluidic devices made out of glass, silicon, or polymers [7, 8]. The evolution of the open-channel electrophoresis was followed by proper mathematical descriptions of the involved phenomena, required for deep understanding of the methods, for prediction of the outcome of experiments, and for rational design of novel electrophoretic devices [9]. One-dimensional CZE, ITP and IEF problems where successfully modeled using non-linear partial differential equations (PDE) describing the charge and mass conservation principles [10]. By using this approach, several software tools have been developed to simulate specific 1D problems [11, 12, 13]. Improvements to these models were reported in the past decade, appealing to more complex formulations for particular physicochemical conditions [14], and electrically-driven flows [15]. Furthermore, particular applications like IEF in nano-channels [16], 2D IEF [17, 18], free-flow IEF (FFIEF) [19], and even FFIEF combined with CZE in a 2D lab-on-a-chip device [20] were successfully modeled with computational tools based on the finite element (FEM) or finite volume (FVM) methods. Also, a commercial FEM tool was recently reported to successfully replicate 1D benchmark problems, with the potential to solve 2D and 3D arbitrary cases [21]. Recently, a comprehensive model was reported, dealing simultaneously with the fluid flow (including EOF), transport, charge conservation, pH and effective mobility problems, in arbitraty 3D geometries [22].

In the last 5 years, electrophoresis on paper substrates regained relevance [23, 24] due to the boom of microfluidic paper based analytical devices (μPADs). μPADs arose as a promising option for rapid, inexpensive, and on-site assays, for environmental monitoring, food safety, and for veterinary and human health [25]. Regarding the last application, μPADs are expected to truly reach the end-user or low trained personnel at sensitive areas like point-of-care, low-resource-settings and remote populations [26]. Thus, paper zone electrophoresis (ZE) has been demonstrated [27, 28] and ZE μPADs have been used for amino-acid [29] and protein separation [30]. Also, ITP on μPADs has been assessed [31, 32] and devices for immunoglobulin [33], nucleotide strands [34, 35] and bacteria detection [36] have been reported.

However, only a few analytical descriptions of electrophoretic μPADs have been reported, limited to one-dimensional channels and the transport of a single chemical species [32, 34] or the binding of an ITP-focused analyte to the reaction zone [33]. Other works provided more complete descriptions, for 2D and 3D geometries including the mechanical dispersion produced by the intricate network of cellulose fibers [37, 38], the reaction kinetics, and the velocity field due to the capillary action [39]. Other authors derived methodological descriptions for fluid flow [40, 41] or transport of chemical species [42] in generic porous materials.

Nevertheless, none of the named reports deals simultaneously with all the relevant phenomena involved in the electromigration of chemical substances in paper substrates, namely: the fluid dynamics including the EOF, the transport of all the chemical species, the acid-base equilibrium, and the electric field distribution in the porous matrix formed by the cellulose fibers. Even more, none of the reports, to the best of our knowledge, includes a transport mechanism to account for the solute dispersion produced by the action of electric fields. Analogously to the fluid flow dispersion [37], the ions forming a plug are expected to be exposed to different velocities, either longitudinally or transversely, due to the cellulose fiber network, causing an *electrophoretically-driven mechanical solute dispersion* (EDMSD). The dispersion produced by EOF has been studied in a previous work [43], but this effect is due to the advective mass transport, and in principle differs from the effect of electrophoretic transport of charged species. Such kind of dispersion, can be observed in experimental works already published [28, 31], and it has even been exploited to improve mixing [44], although theoretical explanations remain to be provided. Therefore, more exhaustive modelling is needed to develop a deeper understanding on μPAD electrophoresis to better design complex configurations such as paper-based free-flow electrophoresis (FFE), FFIEF, and combinations of the different electrophoretic modes, in 2D and 3D formats [45, 46].

In this work, a comprehensive 3D model is presented including PDEs for all the relevant phenomena involved in the transport of chemical species, subject to an electric field in a paper substrate. First, proper scaling laws are introduced to account for the modifications produced in the open-channel equations by the porous media. Then, proper PDEs are derived for hydrodynamic

flow, transport of chemical species and charge conservation. While the foundations for these PDEs can be found in different works, here, the entire set of PDEs is derived methodologically and each PDE is presented accounting for all the phenomena involved. A special case is the EDMSD term, which is introduced here for the first time, to the best of our knowledge. In order to validate the proposed model, we performed numerical simulations of experiments reported in the literature [28, 31]. Finally, the model was used to simulate a challenging case: FFE on Whatman filter paper for the separation of amino acids.

2 Theory

2.1 Mathematical model

The proposed mathematical model was developed under the following set of hypothesis: i) The porous matrix is in principle modelled as a bundle of tortuous capillaries with variable cross sectional area. ii) The geometrical shape of the substrate is constant along the experiments, then, deformation, or swelling effects are not taken into account. iii) Evaporation is not accounted for. This is reasonable for laminated paper substrates, controlled environments and/or short-duration experiments. iv) All the systems and processes are supposed to be isothermal. v) Retention effects such as adsortion, electrostatic wall forces or hydrophobic/hydrophilic interaction, are neglected for the transport of molecules.

2.1.1 Effective medium approach and scaling laws

The differential model presented here, is based on a effective medium approach, in which the different physicochemical magnitudes are computed in an intermediate scale, larger that the pores, but smaller than the modeled domain, such that the porous matrix of the paper can be treated as a continuum. Further analysis of this approach can be found elsewhere [39]. In what follows we outline the scaling laws needed to properly define the physical magnitudes in terms of the macroscopic parameters of the porous medium. Volume scalars in a non-porous material (such as concentrations) can be related to their porous counterpart trough the porosity $\phi = V_{void}/V_{total}$, where V_{void} is the void volume within the substrate whose nominal volume is V_{total}. If a is a volume scalar, then its effective value a_p in the porous medium is:

$$a_p = a\phi \tag{1}$$

where the p subscript denotes paper. The porous medium can be considered as a group of tortuous hollow capillaries embedded in a solid matrix, approximately aligned to the flow direction. Then, the porosity can be rewritten as $\phi = NA_p l_p/AL$, where A and L are the cross-sectional area and length of the matrix, A_p and l_p are the average cross-sectional area and length of the pores and N is the number of capillaries. Defining the average tortuosity $\tau = l_p/L$ and noting that $NA_p = A_{void}$, then $A_{void}/A = \phi/\tau$. This ratio is used to scale flux related quantities. For example, mass conservation requires $uA = u_p A_{void}$, where u is the average flow velocity and u_p is the average flow velocity at the pore level [40]. Then,

$$u_p = u\frac{A}{A_{void}} = u\frac{\tau}{\phi} \tag{2}$$

Finally, the winding nature of the pores has to be taken into account in the calculation of spatial derivatives because the real distance between electric potential Φ and pressure p sources and sinks is,

$$x_p = \tau x \tag{3}$$

in which x is a coordinate in the scale of the porous medium and x_p the corresponding coordinate inside the pores [40].

2.1.2 Generalized Navier-Stokes equation for porous media

The velocity field in porous media can be described with a modified version of the Navier-Stokes equations [47] corrected to describe the average flow through the porous medium by applying the scaling laws 2 and 3. Also, two terms need to be included, accounting for the drag produced by the solid portion of the porous channel, and the electric force over the electrolyte solution, respectively. These modifications yield [40],

$$\begin{aligned} \frac{\tau}{\phi}\frac{\partial \mathbf{u}}{\partial t} + \frac{\tau}{\phi}\mathbf{u}\cdot\nabla\left(\frac{\mathbf{u}}{\phi}\right) &= \frac{\mu}{\rho\tau}\nabla^2\left(\frac{\mathbf{u}}{\phi}\right) - \frac{1}{\rho\tau}\nabla p - \frac{\rho_e}{\rho\tau}\nabla\Phi + \frac{\mu}{\rho}\frac{\mathbf{u}}{K} \\ \nabla\cdot\mathbf{u} &= 0 \end{aligned} \tag{4}$$

where μ is the fluid viscosity, ρ is the fluid density, ρ_e is the charge density of the electrolyte solution and K is the Darcy's permeability of the medium. The third term on the right–hand–side corresponds to the EOF associated to an externally applied electric field $-\nabla\Phi$. The last term on the right–hand–side accounts for the viscous effect produced by the cellulose fibers, which is known as the Forchheimer force, and on a more general form can be written as $\mathbf{F} = \mu\mathbf{u}/\rho K + F_\epsilon\mathbf{u}|\mathbf{u}|/\sqrt{K}$ where F_ϵ is the friction factor. Usually the non–linear contribution can be neglected for the velocities found in microfluidic devices [40]. Also, the left-hand side of eq. 4 can be neglected in stationary problems with low Reynold numbers (usually the case in μPADs) [40], and the Laplacian viscous term can be neglected when compared to $\mathbf{F}$. Then, eqs. 4 simplifies to,

$$\begin{aligned} \frac{1}{\tau}\nabla p + \frac{\rho_e}{\tau}\nabla\Phi &= \frac{\mu}{K}\mathbf{u} \\ \nabla\cdot\mathbf{u} &= 0 \end{aligned} \tag{5}$$

which can be interpreted as a modified Darcy's law that includes electroosmotically-driven flows in porous media. The pressure driven term represents any pressure source, such as capillarity or an external pump. In any case, the proper pressure value (like the Laplace pressure for capillarity [39]) has to be fixed as a boundary condition.

In equations 4 and 5, ρ_e has two contributions: the bulk ion concentration density ρ_e^b and the ion concentration density associated to the electrical-double-layer developed around the surface of the cellulose fibers ρ_e^p. The first contribution vanishes because the bulk fluid is assumed to be electro-neutral, i.e. $\rho_e^b = F\sum z_j c_j = 0$, where F is the Faraday's constant and z_j and c_j are the charge number and concentration of the j-th species respectively [48]. The second contribution is regarded as the (pore cross-sectional area) averaged charge distribution that produces an effective electrically-driven fluid flow [40]. A model for such charge density is,

$$\rho_e^p = \frac{\phi\epsilon\zeta}{\tau K} \tag{6}$$

where ζ is the wall (in our case the cellulose fiber) electrokinetic potential, and ϵ is the electrical permittivity of the fluid [40]. Regarding the ζ-potential, a $\zeta(pH)$ model can be used, as suggested in reference [41]. It is worth noting that in one-dimensional flows, only for the cases of uniform ζ and $-\nabla\Phi$, the EOF velocity can be described by using the Helmoholtz-Smoluchowski's equation [22] modified for porous media, $u_{EOF} = \phi\epsilon\zeta\Delta\Phi/\tau^2\mu l$. This equation can be obtained assuming a pure elecroosmotically-driven flow in eq. 5 (i.e. $\nabla p = \mathbf{0}$) and replacing ρ_e^p value by eq. 6.

In particular, in the experimental cases studied in this work, pH conditions were constant in time and uniform in space, thus we have not considered pH-induced variations of the EOF.

2.1.3 Generalized transport equation for porous media

The transport of a diluted chemical species j through a non-porous channel is described by the mass conservation equation $\partial c^j/\partial t = -\nabla\cdot\left(\mathbf{u}_f c^j - D_0^j\nabla c^j\right) + r^j$ where c^j is the concentration of the species and r^j is its production rate. Two transport mechanisms are present: i) diffusion, being D_0^j the diffusion coefficient and ii) advection, being $\mathbf{u}_f$ the fluid velocity [48]. To adapt this equation to porous media, equations 1, 2 and 3 are used for volume scalars (c and r), velocities, and spatial derivatives, respectively, yielding,

$$\frac{\partial(c^j\phi)}{\partial t} = -\nabla\cdot\left(\mathbf{u}_f c^j - \frac{D_0^j}{\tau^2}\nabla\left(c^j\phi\right)\right) + r^j\phi$$

A similar equation was obtained in [42]. The expression D_0^j/τ^2 can be considered like an effective diffusivity D_p^j of the porous medium. Regarding the advective term, no correction coefficient applies, because the divergence of the mass flux $\mathbf{u}_f c^j$ is increased by the factor τ/ϕ, while decreased by the the winding nature of the path by $1/\tau$ and by the reduced effective concentration by ϕ.

However, other transport mechanisms are present in the studied problem. The pore network introduces an alternating variation of fluid velocity, in both magnitude and direction, producing additional solute dispersion. This effect can be represented by a transport mechanism called mechanical dispersion, producing a mass flux proportional to a dispersivity coefficient s_f and to the average velocity in the porous medium [37].

In an open-channel, under the action of an electric field $-\nabla\Phi$, the charged species j is expected to migrate with a velocity $\mathbf{u}_e = -\Omega^j\nabla\Phi$, where Ω^j is the electrophoretic mobility of such species [48] for the given conditions of pH and ionic strength [22]. Thus, the distance traveled by a charged molecule is $d = \Omega^j t(\Phi_{in} - \Phi_{out})/l$ where t is time, Φ_{in} and Φ_{out} are the electric potentials applied at the inlet and outlet respectively, and l is the distance between the electrodes [2]. In porous media, $\mathbf{u}_e$ has to be corrected taking into consideration that both d and l are affected by scaling law 3, yielding $\mathbf{u}_e = -\Omega^j\nabla\Phi/\tau^2$. Then, the effective mobility in porous media is $\Omega_p^j = \Omega^j/\tau^2$, as proven by [2]. It is worth noting that, even though $\mathbf{u}_e$ is a velocity, the scaling law given by eq. 2 does not apply, since it is valid for fluid velocities and $\mathbf{u}_e$ is the velocity of a charged molecule. This result for Ω_p^j can also be obtained replacing D^j with D_p^j in the Nernst-Einstein equation $\Omega^j = D^j(F/RT)$ [48], where R is the gas constant and T is the temperature.

With this additions, the generalized transport equation for porous media can be written as,

$$\frac{d(c^j\phi)}{dt} = -\nabla\cdot\left(\left(\frac{\mathbf{u}_f}{\phi} + \frac{\Omega^j}{\tau^2}\nabla\Phi\right)(c^j\phi) - \left(\frac{D_0^j}{\tau^2} + s_f|\frac{\mathbf{u}_f}{\phi}| + s_e|\frac{\Omega^j}{\tau^2}\nabla\Phi|\right)\nabla\left(c^j\phi\right)\right) + r^j\phi \qquad (7)$$

where s_e is the dispersivity of the media due to EDMSD, i.e. $s_e|\mathbf{u}_e|$ accounts for the dispersion produced in the concentration field of a charged species, when an electric field is applied. As a first approximation, s_c and s_e are expected to take similar values. In equation 7, it should be noted that $s_f|\mathbf{u_f}|$ was corrected by τ/ϕ and $1/\tau$, in analogy to the convective term. Also, $\mathbf{u}_f$, which already accounts for EOF, can be obtained with equation 4, or 5, while Φ can be obtained with the equation presented next. Also, H^+ concentration field (or pH) and $\Omega_{(pH)}^j$, can be calculated as in reference [22].

It is important to note that chromatographic effects can play a relevant role in paper substrates [49]. The presented formulation does not include chromatographic effects, which are to be considered in future implementations of the model. In particular, all the experimental cases considered in the manuscript involve small inorganic molecules as chemical species (both for analytes and buffer constituents). Such small inorganic ions interact with walls in a way that any retention effect can be neglected due to its low relative magnitude compared with the other considered transport phenomena.

2.1.4 Generalized charge conservation equation for porous media

The electric potential in the bulk fluid of open-channels is calculated through the Gauss' Law $\nabla^2\psi = -\rho_e/\epsilon$ [48]. This total electric potential ψ has two main contributions: i) a ζ potential due to the electric double layer near the walls, which usually decays within around 10 nm and ii) a Φ potential due to an external source. Ideally, $\nabla\zeta \gg \nabla\Phi$ and also $\zeta \perp \Phi$, since the former is perpendicular and the last is tangent to the channel walls, thus both contributions can be treated separately [20]. Because of the length scales involved, solving $\nabla^2\zeta = -\rho_e/\epsilon$ would require a large computational cost, hence it is preferable to deal directly with its effect, the EOF, in the momentum equation [22].

The external contribution Φ can be obtained from the steady-state conservation of charge $\nabla\cdot\mathbf{i} = 0$, where $\mathbf{i}$ is the electrical current density with three contributions of charge flux in open-channels: i) the ohmic current density $-\sigma\nabla\Phi$, being σ the conductivity of the electrolyte solution,

ii) a diffusive contribution $-F\sum_{j=1}^{N} z_j D_0^j \nabla c^j$ and iii) an advective contribution $\rho_e \mathbf{u}_f$, which can be neglected since electroneutrality is assumed in the bulk of the fluid [22, 48].

In the case of porous media, a similar approach can be followed. The two contributions to ψ are also ζ (relevant within 10 nm near the cellulose fibers), and Φ valid in the bulk of the pores. Also, the relations $\nabla\zeta \gg \nabla\Phi$ and $\zeta \perp \Phi$ hold, thus they can be treated separately. The EOF was analyzed in section 2.1.2, while Φ can be calculated from a generalized charge conservation equation for porous media. To obtain such equation, not only the dispersive contribution has to be fixed as in Eq. 7, but also a proper ohmic contribution needs to be derived. The conductivity can be corrected starting from the open-channel conductivity $\sigma = F\sum_{j=1}^{N} z_j^2 \Omega^j c^j$ [48], recalling the effective mobility Ω^j/τ^2 and concentration $c_j\phi$, yielding,

$$\sigma_p = F\sum_{j=1}^{N} z_j^2 \frac{\Omega^j}{\tau^2} c^j \phi = \frac{\phi}{\tau^2}\sigma \tag{8}$$

Again, the conductivity in the averaged porous media can be thought as an effective conductivity σ_p which relates to the open-channel conductivity by $\sigma\phi/\tau^2$. An alternative way to obtain this result is presented in the supplementary information. Several reports relating σ and σ_p have been published [50, 51, 52, 53, 54], most of them based on the Archie's Law, which states that $\sigma_p/\sigma = \phi^m$ [50], where m is obtained empirically and usually $1.3 < m < 2.2$ [51]. These works cover wide porosity ranges [51, 52], and model effects like pore saturation [54] and the existence of bottle necks [52], adding complexities that do not apply for saturated mediums with high ϕ and moderate τ like paper. These reports do not include τ explicitly, with the exception of [51] which arrives to an expression where $\sigma_p/\sigma \propto \phi/\tau^2$. Also, σ_p can be modified to account for the intrinsic ohmic conductivity of the wet (with pure solvent) cellulose fibers, σ_0. With this addition, $\sigma_p = \sigma_0 + \sigma\phi/\tau^2$, as revised in [54]. However, in many applications $\sigma \gg \sigma_0$ and thus σ_0 can be neglected. Finally, the charge conservation equation corrected for paper-like porous media is,

$$\nabla\cdot\left(-\frac{\phi}{\tau^2}\sigma\nabla\Phi - F\sum_{j=1}^{N} z_j\left(\frac{D_0^j}{\tau^2} + s_f\left|\frac{\mathbf{u}_f}{\phi}\right| + s_e\left|\frac{\Omega^j}{\tau^2}\nabla\Phi\right|\right)\nabla(C_j\phi)\right) = 0 \tag{9}$$

where the correction of the divergence operator and $-\nabla\Phi$ are already included in the effective coefficients.

3 Materials and methods

3.1 Numerical resolution of the model

Solving the mathematical problem consists in finding the unknowns $\mathbf{u}_f$, p, c^j and Φ, contained in equations 4, 7 and 9. This system of coupled equations was solved iteratively using the *electroMicroTransport*[22] toolbox for *OpenFOAM*®[55], an open-source tool based on the finite volume method. The hardware employed was a desktop computer with a single quad–core Intel i7 7700 3.6 GHz processor and 16 GB DDR3–2400 memory. The problems were solved in parallel using 4 calculation threads.

4 Results and discussion

4.1 Validation case 1: ZE-μPAD

The numerical model was validated against experimental data found in the literature. The first selected problem is a zone electrophoresis separation reported in [28]. In this example, a 500 μM sodium sample is placed in a 60 mm long, 1 mm width Whatman #1 channel. The injection channel and detector positions are 13 mm and 50 mm, respectively. The original device is sketched in Fig. 1A. BGE is composed of 20 mM MES and 20 mM Histidine (pH = 6.1). Figs. 1B-D present the electropherogram obtained when a 2.5 kV electric potential is applied across the channel.
This problem was solved numerically by using the parameters detailed in the supplementary information. A 60 mm one-dimmensional channel was meshed with 12000 cells, and a 1 mm width

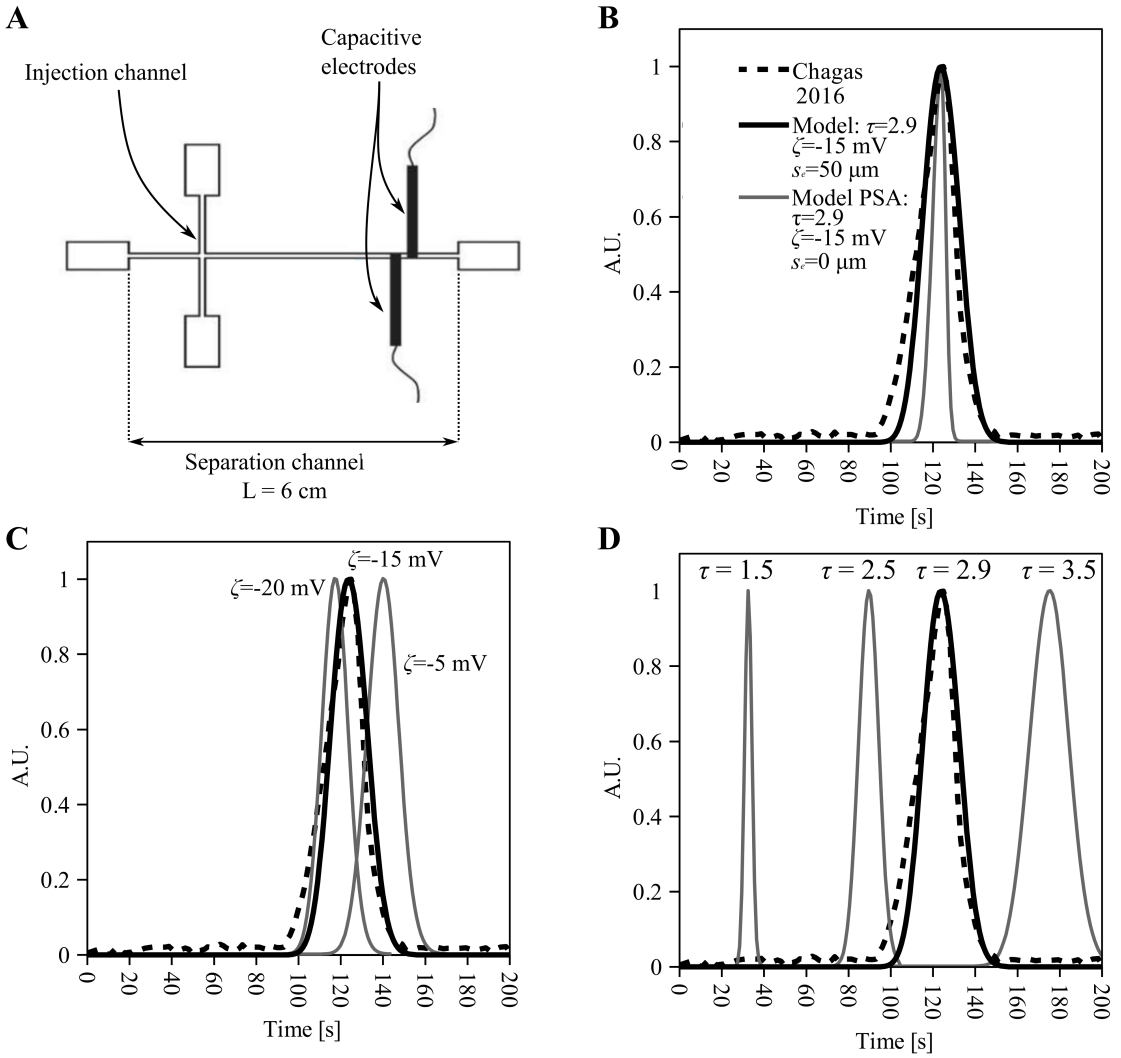

Figure 1: A) Sketch of the electrophoretic device chosen as validation case 1. Modified from [28] and reprinted with with permission from The Royal Society of Chemistry. B) Comparison of the experimental electropherogram obtained with capacitive electrodes (dashed line) and the model electropherogram obtained starting from the sample concentration (solid lines). The best match corresponds to the black-solid line, obtained with τ=2.9, ζ=−15 µV and s_e =50 µm. The gray-solid line is obtained with $s_e = 0$. C) Parametric sensitivity analysis (PSA) on ζ using the maximum and minimum values reported [56]. D) PSA on τ, using the average value τ_{AV} and $\tau_{AV} \pm SD$ given in the supplementary information. Here, sodium peaks were scaled in magnitude to fit the sensor gain.

sample plug was placed in the injection position. The simulation was run until t =200 s giving the results shown in Figs. 1B-D. In these figures, the amplitude of the numerical and experimental results are inversely proportional to the electrical impedance or, equivalently, proportional to the analyte concentration [57]. When the correct set of parameters is used (τ=2.9, ζ=−15 mV, s_e =50 µm), it can be seen how the peak positions coincide almost exactly (error lower than 2%) while the peak widths (characterized as the full width at half maximum or FWHM) also show a low error (lower than 5%). Figure. 1B also shows the effect of neglecting the EDMSD, producing a narrower peak, with an error higher than 60%. PSA on ζ (Fig.1C) and τ (Fig.1D) were also performed, using the extreme values reported for such parameters: $-5\,\text{mV} > \zeta > -20\,\text{mV}$ [56] and $1.5 < \tau < 3.5$ (refer to supplementary material). The PSA on both parameters exhibit great deviations from the experimental peak position, with considerable errors, such as 12% for ζ and 74% for τ, when the extreme values of in variation ranges are used. The large peak shift produced by the variation of τ can be explained by considering that electrophoretic and electroosmotic mobilities

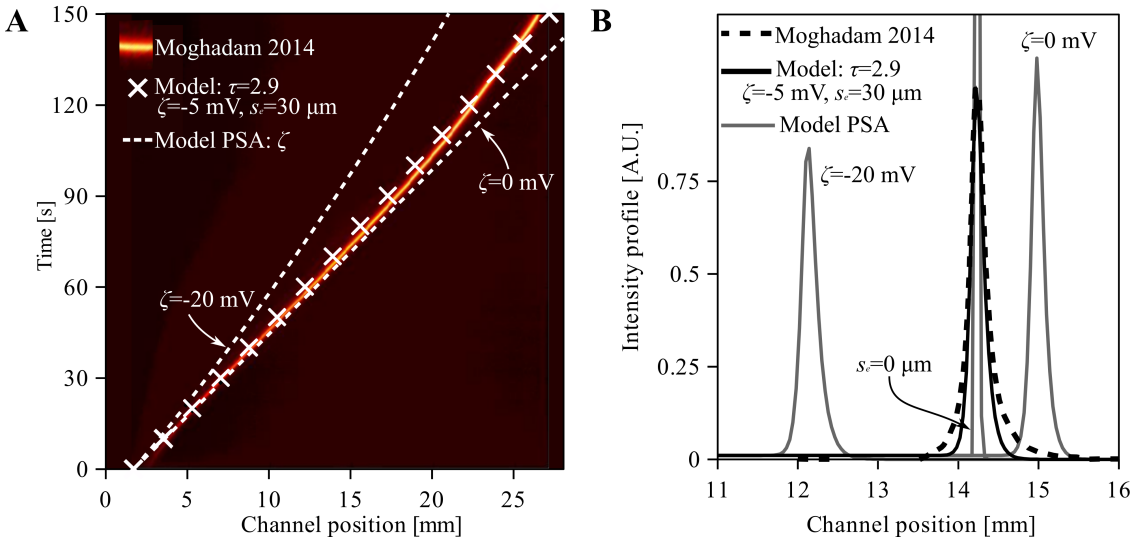

Figure 2: Comparison of experimental [31] and model results for validation case 2. A) Position of the ITP plug over time (Adapted with permission from [31]. Copyright (2014) American Chemical Society). The best model prediction is indicated with cross markers. PSA on ζ is indicated with dashed lines, respectively. PSA on τ was performed but is not indicated since all the curves overlap. B) Normalized experimental Alexa-Fluor intensity profile and concentration profiles predicted by the mathematical model. PSA on ζ and s_e are marked with gray lines.

are both affected by $1/\tau^2$.

4.2 Validation case 2: ITP-µPAD

In the system selected as the second validation case, ITP is performed in a 3.5 mm width and 40 mm long nitrocellulose channel [31]. The leading electrolyte (LE) is composed of 40 mM Hydrochloric acid with 80 mM Tris (pH=8.1), and the trailing electrolyte (TE) is composed of 10 mM HEPES with 20 mM Tris (pH=8.2). The analyte used is 50 nM Alexa-Fluor 488. A 3 % PVP concentration is added to the LE composition for EOF reduction. The sample injection position is approximately x =3 mm. When t =0 s, a 500 µA current is applied obtaining the curves shown in Fig. 2A, for sample plug position versus time, and Fig. 2B, for plug intensity profile (obtained using fluorescence microscopy) versus channel position.

Solutions to the mathematical model for this problem were obtained numerically by meshing the 40 mm one-dimmensional channel with 4000 cells. At each boundary of the channel the concentrations of TE and LE were imposed, to the reservoirs concentration respectively. The simulation was run until t =150 s yielding the results given in Fig. 2. The experimental position along time is overlapped with the model predictions in Fig. 2A, with a small error (lower than 4%) when ζ =−5 mV and s_e =30 µm. The rest of the used parameters is listed in the supplementary information. In Fig. 2B the Alexa-Fluor numerical concentration profile correlates accurately with the experimental intensity profile at t =65 s, with an error lower than 10% in the FWHM. Figure 2 also shows a PSA on τ, ζ and s_e. In the first case, the position of the plug remains unchanged for variations between 1.5 and 3.5. Again, electrophoretic and electroosmotic mobilities are reduced by the same amount ($1/\tau^2$), but the electric field is increased by τ^2/ϕ, as can be deduced from eq. 9, after neglecting the dispersive terms and recalling that current is fixed. The net result is that the effect of τ is cancelled when a constant current is used. On the other hand, ζ-variations only affect EOF, changing the plug position up to $\sim$ 15%. The experimental curve lays between total EOF suppression (ζ=0 V) and EOF for the maximum reported ζ (−20 mV) [56]. Thus, PVP significantly reduces EOF, although it does not achieve total suppression. Finally, neglecting EDMSD, gives a an error in the peak width less than 60%.

4.3 Application case: FFE-μPAD

In FFE, the analytes to be separated are injected continuously into a liquid carrier and an electric field is applied perpendicular to the flow direction. In the separation chamber, analyte molecules are deviated from the flow streamlines in the direction of the vector composition of hydrodynamic and electrophoretic velocities. Thus, the mobilities of the different analyte molecules, produce different deflection angles and reach different zones within the outlet of the separation chamber. Inspired by a previous work [18], a paper-based FFE device for amino acid separation (see Fig. 3A) was numerically prototyped, to demonstrate the full potential of the model for dealing simultaneously with different effects. In this device, capillary action produces an horizontal flow, from the inlet to the two outlets connected to a capillary pump (i.e. an absorbent pad). Also, an electric potential applied across the electrodes produces an electromigrative velocity. After device operation, the separated amino acids can be claimed directly by cutting-out the outlet strips.

It is important to describe here relevant facts about the design and optimization process of the device. As already mentioned, this FFE separation is based on a previous work on modelling and simulation electromigrative phenomena in open-channel microfluidic chips [18]. By using the presented numerical tool, several attempts were performed trying to reproduce the analytical performance of such device. The first obstacle were the original dimensions ($3 \times 1\text{mm}^2$) and fluid velocity which could not be reproduced in a μPAD due to the extreme mixing produced by solute dispersion. This effect generated almost uniform analyte concentrations inside the chamber. In order to deal with this problem, larger dimensions were proposed as a possible solution [58]. After this modification, applying Φ at the inlets and outlets of the device (as in the original open-channel device) was no longer suitable for proper separation, since the electric field in the chamber was highly nonuniform. Therefore, the electrodes were placed along the chamber lateral sides, immersed in a high conductivity buffer, as proposed in reference [59]. Gathering these concepts, a different device was obtained in terms of dimensions and operative conditions, but capable of performing the same FFE separation than the open-channel counterpart. More details about this design process can be found in the supplementary information.

For the final device design, the operation of the FFE-μPAD was simulated by using 90000 250 μm square cells and the parameters listed in the supplementary information. The electric field lines and flow streamlines obtained are depicted in Fig. 3B for a 600 V drop across the electrodes. At the pH of the BGE (6.25), negatively charged aspartic acid from the sample migrates towards the anode and is collected in the upper outlet, while positively charged lysine migrates towards the cathode and is collected in the lower outlet. This is shown in Fig. 3C for different times. Fig. 3D compares simulations undertaken with EDMSD, without EDMSD, and without both dispersion mechanisms. In Fig. 3D, the dispersion associated to both s_f and s_e (lower panel) in the order of millimeters, can be clearly noted. It is clear that the EDMSD makes the major contribution to transverse dispersion and thus, it should not be neglected when modelling.

5 Summary and conclusions

A complete numerical model for the electromigration in μPADs was derived, which is based on equations that describe the motion of fluids by capillary action and EOF (eq. 4), the transport of charged chemical species (eq. 7), and the electric potential distribution (eq. 9). The porous medium was considered like a network of tortuous capillaries and represented by macroscopic parameters following an effective medium approach. Equations 4 (or 5), 7 and 9 form a system of equations to solve four unknowns ($\mathbf{u}_f$, p, c^j, Φ), provided that all the parameters describing the porous medium (ϕ, τ, K, ζ, s_f, s_e), the solvent fluid (μ, ρ, ϵ) and the transported species j (Ω^j, D_0^j, z^j) are given. The three equations were obtained starting from their open-channel counterparts. Proper scaling laws for linear displacements (eq. 3), cross sectional area (eq. 2) and volume quantities (eq. 1) were obtained to adapt bulk fluid transport equations to properly represent transport phenomena in the porous matrix. Although eq. 4 was obtained from literature and most of the terms in eqs. 7 and 9 could be found spread in previous reports, the contribution of this work is the derivation of all these phenomena in a comprehensive form.

Moreover, EDMSD was proposed as a novel transport mechanism. In the validation case 1, not only EDMSD was required to explain the solute dispersion obtained experimentally, but also the required value for s_e was in the order of the tenth of microns, the same already obtained for the mechanical dispersion [37, 45]. This proves that the assumption $s_e \approx s_f$ made in section 2.1.3 was

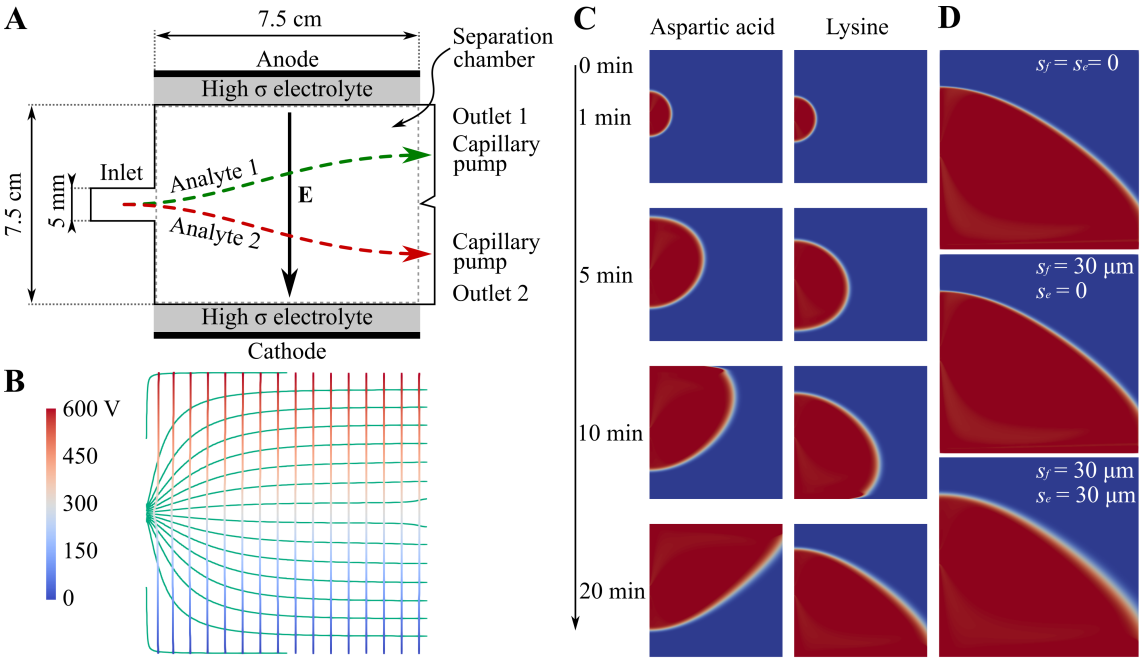

Figure 3: A) Schematic representation of the paper-based FFE device operation (out of scale). The area within the dashed rectangle, is the simulation domain. B) Streamlines of the hydrodynamic flow produced (horizontal) and electric field lines (vertical). The color scale represents Φ along the streamlines. C) Time progress of the analyte concentration fields within the separation chamber. D) Concentration profiles of lysine when: (top) only Brownian diffusion is considered, (middle) mechanical dispersion is also computed and, (bottom) Brownian, mechanical dispersion and EDMSD are accounted for.

reasonable. The same conclusions can be obtained from validation case 2. Even more, very similar errors in the FWHM were obtained in both validation cases, when $s_e = 0$ was used.

Regarding ζ and τ, it can be noted that the scarce available data for those parameters shows great scatter. Perhaps, the low repeatability associated to μPADs is in part due to that scatter.

The PSA on ζ showed considerable variation when the parameter takes its extreme values, in both validation cases. The PSA on τ showed a serious variation on the peak position, when the extreme values were considered in the validation case 1 (section 4.1). However, the same τ-variation in the validation case 2 (section 4.2) produced no effects in the ITP-plug position. It occurs that both electrophoretic and electroosmotic velocities are independent of τ when a constant electric current density is used. This knowledge can be used for reducing the low μPAD repeatably due to τ-value scatter.

An FFE μPAD was successfully designed using solely the mathematical model and its numerical implementation. The device was optimized and a proper set of physicochemical parameters was found for device operation, reaching a similar analytical performance than its open-channel counterpart, but taking advantage of all the benefits of μPADs. Although FFE was performed on paper substrates 70 years ago, with the aid of the numerical tool we found an operative design comparatively (and significantly) smaller and simpler than those reported previously [58, 59].

The presented model successfully replicated both validation cases when the correct set of parameters was used. However, such set is *a priori* unknown and nominal values (refer to table S1 in the supplementary information) present great scatter. Thus, predictions made using the average values should only be taken as a guide, to provide a first approximation on the device performance. The model can be used to assess the robustness of μPADs, by testing their performance under the complete range of parameter values. Future research should focus on characterizing the most commonly used paper types (such as Whatman #1 or nitrocellulose membranes) in order to create reliable μPADs with the aid of the presented model. Another relevant topic to explore, is to include new terms in eq. 7 to account for chromatographic effects due to adsorption, hydrophobic/hydrophilic interactions, electrostatics, among others.

Acknowledgements

This research was supported by CONICET (Grant PIP-0363), ANPCyT (GrantPICT-2016-0640), UTN (Grant PID ASUTNFE0004475), and UNL (Grant CAI+D-78-5012011010010-0), Argentina.

Conflict of interest

All authors declare complete absence of financial/commercial conflicts of interest.

References

[1] Cremer, H., Tiselius, A., et al. *Biochem. Ztschr.*, 1950, 320, 273–283.

[2] Kunkel, H. G. and Tiselius, A. *J Gen Physiol*, 1951, 35, 89–118.

[3] Shapiro, A. L., Viñuela, E., and Maizel Jr, J. V. *Biochem Bioph Res Co*, 1967, 28, 815–820.

[4] Weber, K. and Osborn, M. *J Biol Chem*, 1969, 244, 4406–4412.

[5] Hjertén, S. *Chromat Rev*, 1967, 9, 122–219.

[6] Jorgenson, J. W. and Lukacs, K. D. *Anal Chem*, 1981, 53, 1298–1302.

[7] Harrison, D. J., Fluri, K., Seiler, K., Fan, Z., Effenhauser, C. S., and Manz, A. *Science*, 1993, 261, 895–897.

[8] Ocvirk, G., Munroe, M., Tang, T., Oleschuk, R., Westra, K., and Harrison, D. J. *Electrophoresis*, 2000, 21, 107–115.

[9] Kler, P. A., Posch, T. N., Pattky, M., Tiggelaar, R. M., and Huhn, C. *J Chromatogr A*, 2013, 1297, 204–212.

[10] Bier, M., Palusinski, O., Mosher, R., and Saville, D. *Science*, 1983, 219, 1281–1287.

[11] Hruška, V., Jaroš, M., and Gaš, B. *Electrophoresis*, 2006, 27, 984–991.

[12] Thormann, W., Caslavska, J., and Mosher, R. *J. Chromatogr. A*, 2007, 1155, 154–163.

[13] Bercovici, M., Lele, S. K., and Santiago, J. G. *J. Chromatogr. A*, 2009, 1216, 1008–1018.

[14] Mao, Q., Pawliszyn, J., and Thormann, W. *Anal. Chem.*, 2000, 72, 5493–5502.

[15] Pimenta, F. and Alves, M. A. *arXiv preprint arXiv:1802.02843*, 2018.

[16] Hsu, W.-L., Inglis, D. W., Startsev, M. A., Goldys, E. M., Davidson, M. R., and Harvie, D. J. *Anal. Chem.*, 2014, 86, 8711–8718.

[17] Yoo, K., Shim, J., Liu, J., and Dutta, P. *Electrophoresis*, 2014, 35, 638–645.

[18] Kler, P. A., Dalcin, L. D., Paz, R. R., and Tezduyar, T. E. *Comput Mech*, 2013, 51, 171–185.

[19] Yoo, K., Shim, J., Liu, J., and Dutta, P. *Biomicrofluidics*, 2014, 8, 034111.

[20] Kler, P., Berli, C., and Guarnieri, F. *Microfluid. Nanofluid.*, 2011, 10, 187.

[21] Mikkonen, S., Ekström, H., and Thormann, W. *J. Chromatogr. A*, 2018, 1532, 216–222.

[22] Damián, S. M., Schaumburg, F., and Kler, P. A. *Comput Phys Commun*, 2018.

[23] Salentijn, G. I., Grajewski, M., and Verpoorte, E. *Anal Chem*, 2018, 90, 13815–13825.

[24] Adkins, J., Boehle, K., and Henry, C. *Electrophoresis*, 2015, 36, 1811–1824.

[25] Gong, M. M. and Sinton, D. *Chem Rev*, 2017, 117, 8447–8480.

[26] Wong, R. and Tse, H. *Lateral flow immunoassay*. Springer Science & Business Media, 2008.

[27] Xu, C., Lin, W., and Cai, L. *J Chem Educ*, 2016, 93, 903–905.

[28] Chagas, C. L., deSouza, F. R., Cardoso, T. M., Moreira, R. C., daSilva, J. A., deJesus, D. P., and Coltro, W. K. *Anal Methods-UK*, 2016, 8, 6682–6686.

[29] Ge, L., Wang, S., Ge, S., Yu, J., Yan, M., Li, N., and Huang, J. *Chem Commun*, 2014, 50, 5699–5702.

[30] Luo, L., Li, X., and Crooks, R. M. *Anal Chem*, 2014, 86, 12390–12397.

[31] Moghadam, B. Y., Connelly, K. T., and Posner, J. D. *Anal. Chem.*, 2014, 86, 5829–5837.

[32] Rosenfeld, T. and Bercovici, M. *Lab Chip*, 2014, 14, 4465–4474.

[33] Moghadam, B. Y., Connelly, K. T., and Posner, J. D. *Anal Chem*, 2015, 87, 1009–1017.

[34] Rosenfeld, T. and Bercovici, M. *Lab Chip*, 2018, 18, 861–868.

[35] Li, X., Luo, L., and Crooks, R. M. *Lab Chip*, 2015, 15, 4090–4098.

[36] Schaumburg, F., Carrell, C., and Henry, C. S. *Anal Chem*, 2019.

[37] Urteaga, R., Elizalde, E., and Berli, C. L. *Analyst*, 2018.

[38] Schaumburg, F., Urteaga, R., Kler, P. A., and Berli, C. L. *J Chromatogr A*, 2018, 1561, 83–91.

[39] Schaumburg, F., Kler, P. A., and Berli, C. L. *Sensors and Actuators B: Chemical*, 2018, 259, 1099–1107.

[40] Scales, N. and Tait, R. N. *J Chem Phys*, 2006, 125, 094714.

[41] Di Fraia, S., Massarotti, N., and Nithiarasu, P. *Int J Numer Method H*, 2018, 28, 472–497.

[42] Shapiro, A. P. and Probstein, R. F. *Envir Sci Tech*, 1993, 27, 283–291.

[43] Li, S., Raoof, A., and Schotting, R. *J Hydrol*, 2014, 517, 1107–1113.

[44] Dey, R., Kar, S., Joshi, S., Maiti, T. K., and Chakraborty, S. *Microfluid Nanofluid*, 2015, 19, 375–383.

[45] Mora, M. F., Garcia, C. D., Schaumburg, F., Kler, P. A., Berli, C. L. A., Hashimoto, M., and Carrilho, E. *Anal Chem*, 2019.

[46] Fu, E., Liang, T., Spicar-Mihalic, P., Houghtaling, J., Ramachandran, S., and Yager, P. *Anal Chem*, 2012, 84, 4574–4579.

[47] Bruus, H. *Theoretical microfluidics*, volume 18. Oxford university press Oxford, 2008.

[48] Probstein, R. *Physicochemical Hydrodynamics. An Introduction.* Wiley-Interscience, 2nd edition, 2003.

[49] Ota, R., Yamada, K., Suzuki, K., and Citterio, D. *Analyst*, 2018, 143, 643–653.

[50] Archie, G. E. et al. *T Soc Petrol En AIME*, 1942, 146, 54–62.

[51] Owen, J. et al. *J Petrol Technol*, 1952, 4, 169–174.

[52] Roberts, J. N. and Schwartz, L. M. *Phys Rev B*, 1985, 31, 5990.

[53] Martys, N. and Garboczi, E. *Phys Rev B*, 1992, 46, 6080.

[54] Ewing, R. and Hunt, A. *Vadose Zone J*, 2006, 5, 731–741.

[55] OpenFOAM. https://www.openfoam.com/. Accessed: 2018-03-19.

[56] Leung, V., Shehata, A.-A. M., Filipe, C. D., and Pelton, R. *Colloid Surface A*, 2010, 364, 16–18.

[57] Brito-Neto, J. G. A., Fracassi daSilva, J. A., Blanes, L., and doLago, C. L. *Electroanal*, 2005, 17, 1198–1206.

[58] Durrum, E. L. *J Am Chem Soc*, 1951, 73, 4875–4880.

[59] Grassmann, W. and Hannig, K. *Naturwissenschaften*, 1950, 37, 397–397.